ENVIRONMENTAL RESEARCH
LETTERS

LETTER • **OPEN ACCESS**

Large-scale circulation-conditioned attribution of the historic 2024 Spanish extreme precipitation

To cite this article: Mengyuan Yao *et al* 2026 *Environ. Res. Lett.* **21** 144026

ENVIRONMENTAL RESEARCH
LETTERS

Check for updates

OPEN ACCESS

RECEIVED
20 April 2026

REVISED
29 June 2026

ACCEPTED FOR PUBLICATION
15 July 2026

PUBLISHED
23 July 2026

LETTER

Large-scale circulation-conditioned attribution of the historic 2024 Spanish extreme precipitation

Mengyuan Yao[1,2] , **Haosu Tang**[3,*] , **Gang Huang**[1,2,*] and **Jun Wang**[4]

1 Key Laboratory of Earth System Numerical Modeling and Application, Institute of Atmospheric Physics, Chinese Academy of Sciences, Beijing, People's Republic of China
2 University of Chinese Academy of Sciences, Beijing, People's Republic of China
3 School of Geography and Planning, University of Sheffield, Sheffield, United Kingdom
4 Key Laboratory of Land Surface Pattern and Simulation, Institute of Geographic Sciences and Natural Resources Research, Chinese Academy of Sciences, Beijing, People's Republic of China
* Authors to whom any correspondence should be addressed.

E-mail: haosu.tang@sheffield.ac.uk and hg@mail.iap.ac.cn

Keywords: extreme precipitation, atmospheric circulation variability, anthropogenic climate change, large ensemble attribution, Mediterranean flood extremes, Cut-off low dynamics, circulation analog

Supplementary material for this article is available online

Abstract

On 29 October 2024, Turís, Spain, recorded an unprecedented 24 h precipitation total of 771 mm, triggering one of the deadliest floods in Europe since 1900. Although recent attribution studies demonstrated that anthropogenic warming may have contributed to the event, the extent to which atmospheric circulation variability shaped its exceptional magnitude remains unclear. Using multi-source high-resolution precipitation observations, this study uncovers the dynamical and thermodynamical mechanisms driving the event. The exceptional precipitation was initiated by an anomalously deep upper-level cut-off low over southern Spain, accompanied by a southeasterly jet that enhanced the transport of warm, moisture-laden air from the Mediterranean. Circulation analog analysis reveals that pre-trough dynamics explain ∼31% (interquartile range: 7%–44%) of the maximum daily precipitation across eastern Spain during October–November 2024. Large-ensemble attribution using the HadGEM3-A-N216 model further confirms the crucial role of internal dynamics, which account for approximately one-third of the total anomaly, while the remaining signal is dominated by the combined contribution of anthropogenic forcing and internal thermodynamic processes. These results highlight the important role of atmospheric circulation in shaping Mediterranean precipitation extremes, emphasizing the need for explicitly accounting for circulation variability in event attribution and future regional flood risk assessment.

1. Introduction

October 2024 witnessed the deadliest flood disaster in Spain since 1973, ranking among the ten deadliest floods in Europe since 1900 (Charalampous *et al* 2025). On 29 October 2024, torrential precipitation triggered catastrophic flash floods across the province of Valencia, with 771 mm recorded within 24 h in Turís (Valencia), including 185 mm within a single hour, setting a national seasonal record (Barriopedro *et al* 2025). The event caused more than 220 fatalities, displaced thousands of residents, and led to economic losses exceeding €13 billion (Charalampous *et al* 2025, Franch-Pardo *et al* 2025). Such impacts are particularly severe in Spain. Between 2000 and 2022, floods accounted for ∼20% of all natural disaster fatalities, while compensation exceeded €7.89 billion, equivalent to 70.5% of the country's disaster-related losses from 1987 to 2023 (Charalampous *et al* 2025). Against this backdrop, the exceptional severity of the October 2024 event raises urgent questions regarding the relative roles of atmospheric circulation variability and anthropogenic warming, highlighting the need for a quantitative, process-based attribution.

In recent decades, both the frequency and intensity of precipitation extremes have increased globally, including across Europe, largely driven by anthropogenic forcing (Kundzewicz *et al* 2017, Masson-Delmotte *et al* 2021, Seneviratne *et al* 2023). This intensification is broadly consistent with thermodynamic expectations under global warming, whereby increased atmospheric moisture availability enhances precipitation extremes and associated flood risks (Kundzewicz *et al* 2017, Robinson *et al* 2021, Yao *et al* 2026). Mediterranean regions have experienced a marked intensification of short-duration convective precipitation (Llasat *et al* 2021, Treppiedi *et al* 2022), highlighting a growing divergence between mean-state drying and extreme-event amplification. Over Spain, anthropogenic forcing has already altered both mean and extreme precipitation characteristics, with projections pointing to increased frequency of intense daily precipitation in the Mediterranean sector (Tramblay and Somot 2018, Cortès *et al* 2019). In addition, flood seasonality has shifted toward later occurrences (Blöschl *et al* 2017, Cramer *et al* 2018), while precipitation distributions have become more variable and heavy-tailed under rising greenhouse gas emissions (Tapiador *et al* 2007, Guerreiro *et al* 2017). Although long-term trends in mean precipitation remain uncertain and their attribution debated (Polade *et al* 2017, Peña-Angulo *et al* 2020, Tarín-Carrasco *et al* 2025), there is growing evidence that anthropogenic warming might intensify individual extreme precipitation events, although confidence remains low (Nojarov 2017, Barriopedro *et al* 2025, Calvo-Sancho *et al* 2026). Yet, catastrophic precipitation is typically triggered by favorable atmospheric circulation configurations and enhanced atmospheric moisture availability, making the relative contributions of dynamical variability and thermodynamic amplification particularly challenging to quantify.

Beyond anthropogenic forcing, large-scale atmospheric circulation exerts a fundamental control on precipitation variability over Spain. The Spanish hydroclimate is strongly modulated by several dominant climate modes, such as the North Atlantic Oscillation and Arctic Oscillation, which influence moisture transport and storm-track positioning (Krichak *et al* 2014). Long-term circulation changes, including a poleward expansion of the Hadley circulation, have also been proposed to shift storm tracks northward, promoting drier conditions across Mediterranean climates (Johanson and Fu 2009, Chang *et al* 2012, Grise and Davis 2020, Tarín-Carrasco *et al* 2025). At synoptic scales, cut-off lows (COLs) play a critical role in shaping extreme hydroclimatic events along the Spanish Mediterranean coast, accounting for approximately one-third of catastrophic flood events, exemplified by the September 2019 Valencia–Murcia event, during which a COL positioned over western Iberia and the adjacent Atlantic intensified precipitation over Valencia. These systems are typically accompanied by anomalous easterly moisture transport from the Mediterranean and enhanced orographic uplift along the Iberian Mountains, favoring intense convective development (Durán *et al* 2013, Ferreira 2021). Consequently, eastern Spain, particularly Valencia, situated on the eastern flank of the Iberian Peninsula, is particularly susceptible to hazardous precipitation and flash-flood events (Insua-Costa *et al* 2021).

Although anthropogenic forcing has been found to increase the likelihood and intensity of the 2024 Spanish flood relative to a pre-industrial climate (Calvo-Sancho *et al* 2026), recent multi-method attribution analyses detect no robust dynamical influence on the event probability and further suggest that circulation variability may obscure the detection of thermodynamic signals (Barriopedro *et al* 2025). However, the absence of a detectable dynamical influence does not imply a negligible dynamical contribution to the observed event intensity itself. To address this gap, we develop an ensemble constructed circulation analog (ECCA) framework to quantitatively decompose the observed precipitation anomaly into contributions of large-scale dynamical variability and potential thermodynamic processes. The framework is applied to both regional mean precipitation and station-based precipitation extremes in southeastern Spain (SES) to provide a more process-based understanding of the circulation conditions underlying the event. Furthermore, we constrain the dynamical conditions using large-ensemble simulations from the HadGEM3-A-N216 attribution system, driven by observed 2024 sea surface temperatures (SSTs) and sea-ice concentrations, to independently assess the contribution of internally generated circulation variability to the extreme precipitation event.

2. Data and methods

2.1. Data

This study primarily uses the Multi-Source Weighted-Ensemble Precipitation (MSWEP) dataset (Beck *et al* 2019), which provides 3 h and daily precipitation at $0.1^\circ \times 0.1^\circ$ spatial resolution from 1979 to the present. MSWEP combines gauge, satellite, and reanalysis data, and applies bias correction using daily and monthly records from more than 70 000 stations worldwide, ensuring high reliability for analyses of both spatial and temporal precipitation variability. Meanwhile, four additional daily precipitation datasets are also explored, including Fifth-generation ECMWF atmospheric reanalysis (ERA5) (Hersbach *et al* 2020), the global precipitation measurement (GPM) Integrated Multi-satellite Retrievals for GPM (IMERG) Final Precipitation V07 (Huffman *et al* 2024), Climate Prediction Center Unified Gauge-Based Analysis of Daily Precipitation (CPC) (Xie *et al* 2010), and the ENSEMBLES daily gridded observational dataset in Europe (E-OBS) (Cornes *et al* 2018). In parallel, *in situ* daily station-based precipitation observations from the Agencia Estatal de Meteorología (AEMET), the State Meteorological Agency of Spain, are used for independent validation. Observed SST fields are derived from the Hadley Centre Sea Ice and SST dataset (HadISST) (Rayner *et al* 2003). Additionally, large-scale atmospheric circulation is obtained from two global reanalysis products: ERA5 (Hersbach *et al* 2020), available for 1979–2024 at a horizontal resolution of $0.5° \times 0.5°$, and the Japanese Reanalysis for Three Quarters of a Century (JRA-3Q) (Japan Meteorological Agency 2023), covering the same period with a horizontal resolution of $1.25° \times 1.25°$. ERA5 serves as the primary dataset for circulation and three-dimensional cloud microphysical diagnostics, given its high spatial-temporal resolution and assimilation consistency, while JRA-3Q is employed to assess data uncertainty and robustness.

To disentangle the contributions of internal variability and external forcing to the extreme event, we employ large-ensemble atmospheric simulations from the HadGEM3-A-N216 model within the Met Office Hadley Centre attribution system (Ciavarella *et al* 2018). The model is run at a horizontal resolution of $0.56° \times 0.83°$ (N216 spectral truncation) with 85 vertical levels. Two ensembles are analyzed. The first is the historical experiment, comprising 15 ensemble members spanning 1960–2013 and driven by observed SST and SIC from HadISST, together with both anthropogenic and natural forcings. The second is the HistExt-2024 experiment, a 525-member ensemble forced by observed 2024 SST and SIC conditions. By perturbing key physical parameterizations, including convection, radiation, and cloud processes, this ensemble samples both internal variability and parameter uncertainty, thereby substantially broadening the range of possible atmospheric states under identical boundary forcing. Within this framework, the externally forced component is estimated from the ensemble mean of the model simulations, which suppresses internal variability and isolates the forced response. The internal variability component is then quantified as the residual between either observations or individual model realizations and the externally forced estimate. Before analysis, all model outputs are bilinearly interpolated onto a $0.5° \times 0.5°$ grid.

2.2. ECCA approach

To separate the dynamic and thermodynamic contributions to the October 2024 extreme precipitation event in SES, we apply the ECCA framework (Guo *et al* 2019, Qian *et al* 2022, Zhang *et al* 2023). It assumes that large-scale circulation exerts a dominant control on regional precipitation patterns, while deviations between circulation-conditioned estimates and observations mainly reflect the unexplained portion of the dynamics, including thermodynamic feedbacks and externally forced responses. Here, we use the zonal gradient of 500 hPa geopotential height (d_xZ500) as the primary circulation metric, as it effectively captures the pre-trough configuration east of Iberian Peninsula with extreme precipitation in the study region (see Results). Circulation analogs are identified based on the spatial similarity of d_xZ500 fields between the target day and historical samples. The corresponding circulation anomaly is reconstructed as a weighted linear combination of the selected analogs:

$$d_xZ500_{\mathrm{OBS}} = \sum_{i=1}^{N} \beta_i d_xZ500_{Ai} + a \tag{1}$$

where d_xZ500_{OBS} and d_xZ500_{Ai} are the observed d_xZ500 on the target day and the d_xZ500 from selected ith analog, respectively. The weights β_i are estimated using ridge regression, whose regularization reduces multicollinearity among analog predictors and improves reconstruction stability:

$$\underset{\beta}{\operatorname{argmin}} \, (y - X\beta)^{\mathrm{T}} (y - X\beta) + \lambda \beta^{\mathrm{T}} \beta \tag{2}$$

where the regularization parameter λ controls the penalty imposed on large coefficients.

The same regression coefficients obtained from circulation reconstruction are subsequently applied to precipitation fields associated with the analog days. This procedure yields the precipitation component that is dynamically consistent with the observed circulation anomaly ($\mathrm{precip_{dyn}}$):

$$\mathrm{precip_{dyn}} = \sum_{i=1}^{N} \beta_i \times \mathrm{precip}_{Ai}. \tag{3}$$

The residual between observation ($\mathrm{precip_{OBS}}$) and $\mathrm{precip_{dyn}}$ is then defined as

$$\mathrm{precip_{res}} = \mathrm{precip_{OBS}} - \mathrm{precip_{dyn}} \tag{4}$$

where $precip_{res}$ represents the component not explained by circulation variability. Following previous ECCA studies (Smoliak *et al* 2015, Singh *et al* 2023), this residual is interpreted primarily as thermodynamic feedbacks and externally forced responses with unresolved dynamical contributions and model bias relative to observations. A schematic summary of the decomposition framework is provided in figure S1.

In the main experiments, we use 15 analog days ($N = 15$) and set the regularization parameter to $\lambda = 0.5$. Sensitivity experiments that vary both parameters produce similar dynamical reconstructions and attribution results (see Results).

The same framework is further extended to the HistExt-2024 large ensemble simulations. The circulation-conditioned reconstruction is applied to internally generated variability, which is further decomposed into internally generated dynamical variability and a residual internal thermodynamic component. Differing from the observation, the analog pool of large ensembles is constructed from internally generated d_xZ500 anomalies across ensemble members and years whose circulation patterns exhibit significant spatial correlations with the observed target circulation pattern. Random sampling from this circulation pool is repeated 1 000 times to estimate the distribution of plausible internally generated dynamical precipitation anomalies. The total thermodynamic contribution is subsequently defined as the sum of externally forced responses and internally generated thermodynamic variability.

To ensure robustness, the ECCA analysis is repeated using ERA5 and JRA-3Q reanalyzes, multiple circulation domains, and four similarity metrics including Euclidean distance, Pearson correlation, Spearman correlation, and cosine similarity. Three spatial domains are defined as D1 (6° W–5° E, 26°–43° N), D2 (5° W–3° E, 28°–41° N), and D3 (3° W–1° E, 29°–38° N). To reduce dependence between analog samples, five non-consecutive-day pools are constructed (e.g. days 0, 5, 10, …), resulting in 120 independent reconstructions. The uncertainty range is defined by the interquartile range (25th–75th percentile) across all realizations.

2.3. Self-organizing map (SOM) analysis

The SOM method serves as an unsupervised machine learning technique for investigating circulation regimes conducive to extreme weather events, providing a potential reference for future extreme precipitation forecasts (Swales *et al* 2016, Zhang *et al* 2022). In this study, the SOM method is used to classify circulation patterns based on d_xZ500. The analysis focuses on clustered daily d_xZ500 fields during October–November from 1979 to 2024 over the domain 15° W–5° E and 32–47° N, encompassing the whole Iberia. Testing various SOM node arrays, including 4×1, 5×1, and 6×1, we find that a 5×1 node SOM is sufficient to capture the range of large-scale circulation patterns, with spatial correlation coefficients (SCCs) between each SOM pattern and its corresponding composite exceeding 0.59 for all SOM nodes.

2.4. Definition of return period

Return periods of the 2024 event, or of a given precipitation threshold, are estimated by fitting a right-tailed Gumbel distribution to the annual time series from 1979 to 2024 ($n = 46$), with parameters derived via maximum likelihood estimation. For the station observations at Turís, a lognormal distribution is fitted to wet-day precipitation amounts (>1 mm). In both cases, goodness of fit is evaluated using the Kolmogorov–Smirnov test at the 95% confidence level. Exceedance probabilities are then derived from the fitted cumulative distribution function, and the return period is defined as the reciprocal of the exceedance probability: $Return\ Period = 1/(1 - CDF)$. Uncertainty of return period is quantified using 1 000 bootstrap resamples, and sensitivity tests using Generalized Extreme Value distributions yield consistent estimates.

3. Results

3.1. Evolution of the October 2024 Spain precipitation extreme

Figure 1 places the October 2024 Spain precipitation event in a global context by comparing daily precipitation on 29 October, corresponding to the onset of the first flood peak (figure S2), with the October–November maximum 1 d precipitation (Rx1day) across global land areas based on the MSWEP dataset. The results demonstrate that the 2024 event ranks among the most extreme worldwide in both daily precipitation intensity and the Rx1day magnitude, contributing substantially to the zonal precipitation belt in the mid-latitudes (figure 1). In Turís (Valencia; red circle in figure 2(b)), 24 h precipitation records reached 771 mm on 29 October 2024, including 185 mm within a single hour, setting a new national record for the autumn season (figures 2(a) and S2). A secondary precipitation peak occurred on 13 November 2024, though with a markedly smaller total of 30 mm. Neighboring stations 8309X and 8395X (black circles in figure 2(b)) also reported exceptionally high values of 215 mm and 175 mm, respectively, on 29 October, though less than one-third of the Turís total (figure 2(a)). This pronounced spatial gradient indicates the highly localized and convective nature of the event and implies limitations of gridded precipitation products in representing sub-grid-scale extremes (figure S3). Despite these challenges, the MSWEP dataset used in this study exhibits strong consistency with the AEMET station network, though it reports a lower maximum grid-point precipitation of 158 mm on that day. MSWEP integrates bias corrections using daily and monthly observations from over 70 000 gauges worldwide and offers a spatial resolution of $0.1° \times 0.1°$, allowing a more detailed representation of the event than most other reanalysis products (figures S2–3). The spatial distribution reveals precipitation maxima concentrated over southern and eastern Spain (figure 2(b)), and the flood-affected areas in SES exhibit multi-peak responses on the days corresponding to the precipitation maxima, closely following the evolution of daily precipitation (figure 2(c)).

Given the short duration and extraordinary intensity of the event on 29 October, the annual Rx1day in October–November is used to assess its historical rarity. The SES-averaged Rx1day (6°–0.5° W, 36°–40.5° N) reached an unprecedented 31 mm, while the eastern sector (5°–0.5° W, 39°–40.4° N) experienced much higher values, reaching 49 mm. In contrast, the southern sector (6°–4° W, 36°–37.5° N)

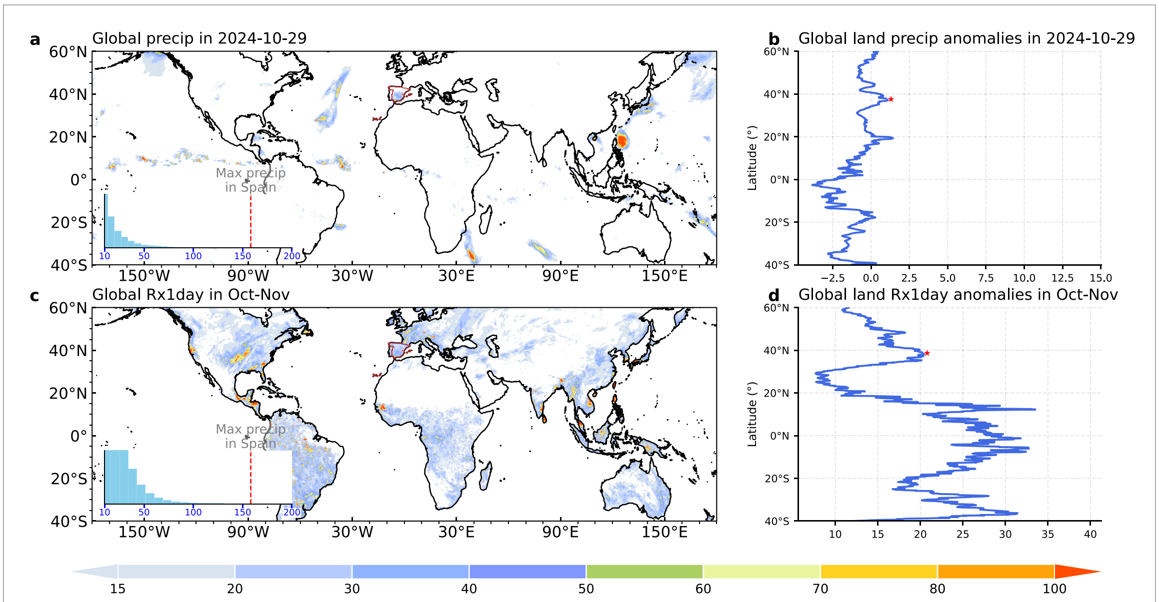

Figure 1. Global precipitation anomalies and their zonal-mean structure on 29 October 2024. (a) Global daily precipitation anomalies on 29 October 2024 derived from the MSWEP dataset. The inset shows the corresponding frequency histogram. (b) Zonal mean distribution of land precipitation anomalies. (c) and (d) Same as (a) and (b), but for global land Rx1day during October–November 2024. In (a) and (c), the red vertical lines mark the maximum precipitation over southeastern Spain (SES), while in (b) and (d), the red pentagrams indicate the latitude of the maximum over SES.

recorded values around 40 mm, which fall within the local historical range (figure 2(d)). Therefore, subsequent analyses focus primarily on eastern Spain. Additionally, given the pronounced spatial heterogeneity of precipitation during the 2024 event, return periods are estimated based on both area-averaged and station-based approaches. For eastern Spain, the area-mean Rx1day yields a return period of ∼100 years (interquartile range: 76–189 years), increasing to 133 years (interquartile range: 98–287 years) when the 2024 value is excluded (figure 1(e)). At the Turís station, the return period for wet-day precipitation (>1 mm), calculated to avoid artificial inflation arising from the dominance of no-rain days in Mediterranean climates, exceeds 10 000 years, underscoring the exceptional nature of the 2024 event (figure 2(e)).

3.2. Synoptic circulation associated with the 2024 Spain flood event

To elucidate the physical mechanisms underlying the extreme precipitation intensity, figure 3 illustrates the temporal evolution of key dynamic and thermodynamic variables from 27 to 30 October, averaged over 1.75°–0.5° W and 39.25°–40° N, the core precipitation zone. Dynamically, mid-to-upper level tropospheric ascent anomalies emerged before 12:00 UTC on 29 October and subsequently deepened to span the entire troposphere during the afternoon. This vertical development was accompanied by pronounced upper-level convergence near 250 hPa and low-level divergence (figures 3(a) and (b)). These dynamical features supported the intensification and eastward shift of the precipitation center toward Valencia, resulting in persistent heavy precipitation until 00:00 UTC on 30 October (figure S2). Thermodynamically, enhanced instability was driven by the co-occurrence of two upper-level cold centers and abundant low-level moisture on 29 October, facilitating the progressive intensification of precipitation (figures 3(c) and (d) and figure S2). Precipitation formes in clouds through two primary pathways: the warm-rain process and the cold, ice-crystal processes (Gupta *et al* 2023). In the lower troposphere, the rapid increase in liquid water content after 12:00 UTC reflected the dominance of the warm-rain pathway, contributing to the rapid and convective intensification of precipitation (figures 3(e)–(h)). In contrast, substantial increases in mid- to upper-tropospheric ice and snow water content after 06:00 UTC promoted the delayed and persistent strengthening of precipitation (figures 3(f)–(h)), through the Wegener–Bergeron–Findeisen process that linked to the cold formation pathway (Omanovic *et al* 2024). This process involves the growth of ice crystals at the expense of supercooled droplets, leading to partial or full cloud glaciation. Such vigorous mixed-phase microphysical processes have been shown to amplify extreme precipitation events (Gupta *et al* 2023, Shi *et al* 2025).

On the synoptic scale, a pronounced COL developed over southern Spain, establishing a strong mid-tropospheric zonal geopotential height gradient that channeled warm and moisture-laden air from the Mediterranean into SES (figures 4(a) and (b)). During the peak of the 2024 flood event (29 October), an intense and persistent southeasterly jet continuously transported Mediterranean moisture toward Valencia (figure 4(b)). As this moist airflow encountered the eastern coastal orography, it was forced to

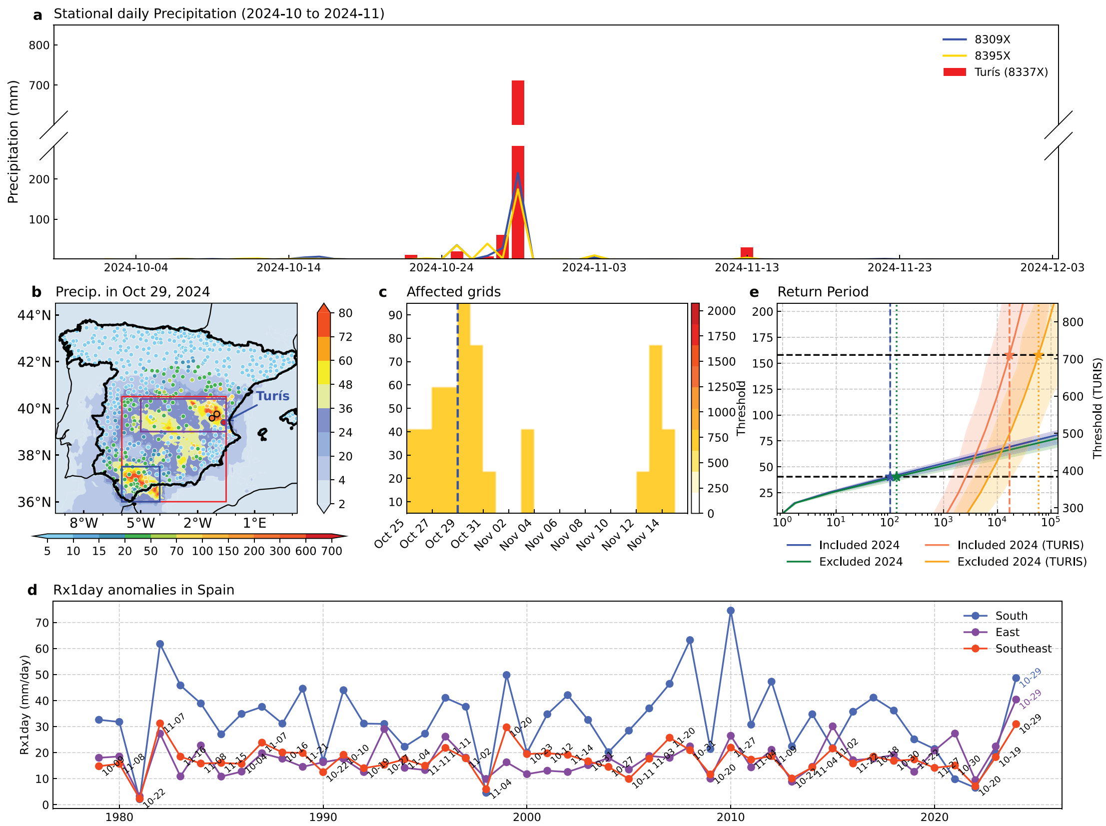

Figure 2. Temporal evolution and spatial characteristics of the 29 October 2024 extreme precipitation event in Spain. (a) Daily precipitation evolution at stations 8309X (Utiel), 8395X (Chelva), and Turís (8337X). (b) Spatial distribution of daily precipitation on 29 October 2024. The red box denotes SES, while the blue and purple boxes represent southern and eastern Spain, respectively. The color bars on the right and bottom correspond to gridded and station data, respectively. (c) Evolution of flood-affected areas (unit: number of 0.1° × 0.1° grid cells; shading) where daily precipitation exceeds the thresholds indicated on the y-axis during the 2024 event. The dashed blue vertical line marks 29 October. (d) Temporal evolution of Rx1day in SES, southern, and eastern Spain. Dates indicate the occurrence of the annual Rx1day in October–November. (e) Return periods of annual Rx1day in eastern Spain and at the Turís station, with the interquartile range estimated from 1 000 bootstrap resamples. Blue dashed and green dotted vertical lines denote return periods calculated with and without inclusion of the 2024 event based on MSWEP, respectively, while the orange and yellow lines are based on the stational records at the Turís station.

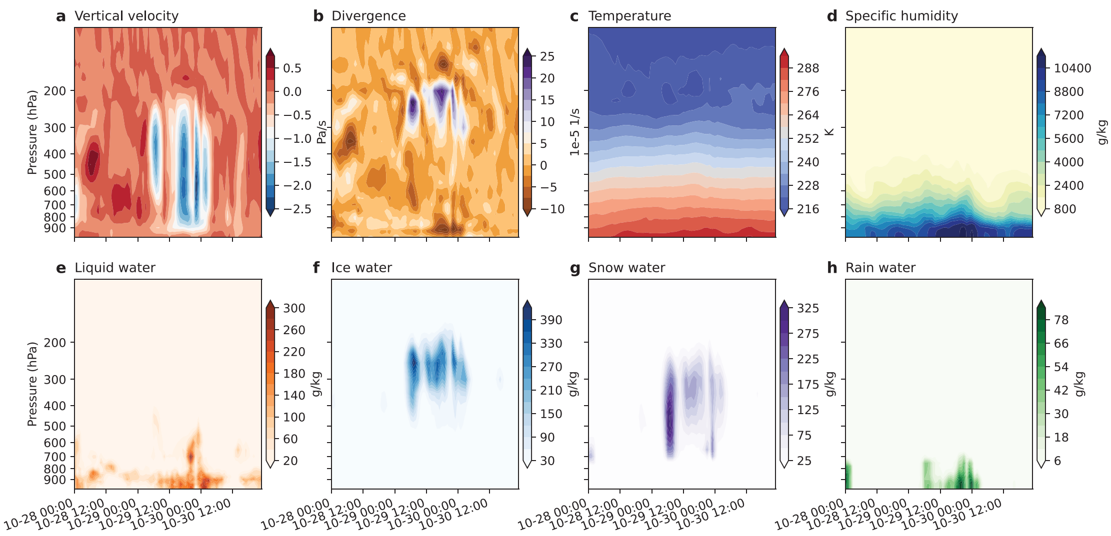

Figure 3. Hourly temporal evolution of dynamic and thermodynamic variables during the 2024 extreme precipitation event. (a)–(h) Hourly time evolution of key atmospheric variables averaged over 1.75°–0.5° W and 39.25°–40° N from 28 to 30 October 2024. (a) Vertical velocity (Pa s^{-1}); (b) divergence/convergence (Pa s^{-1}); (c) temperature (K); (d) specific humidity (10^{-5} s^{-1}); (e) liquid water content; (f) ice water content (g kg^{-1}) (g kg^{-1}); (g) snow water content (g kg^{-1}); and (h) rain water content (g kg^{-1}).

ascend, enhancing vertical motion and latent heat release and thereby further intensifying precipitation (figures 3, 4 and S4). Concurrently, elevated Mediterranean SST anomalies enhanced atmospheric moisture availability and supported sustained ascent, promoting the formation of dense, moisture-rich cloud systems that potentially amplified the precipitation extreme (figure 4(c)). Additionally, the pre-trough configuration over the eastern Iberian Peninsula indicates that vertical motion played a dominant role relative to specific humidity in modulating the 2024 Rx1day (figure S5(a)). When the 2024 event is included, the relationship between Rx1day in eastern Spain and the dynamic factor of d_xZ500 over SES becomes substantially stronger, approximately doubling compared to the relationship obtained when the event is excluded (figure S5(b)).

Given the prominent role of COLs in shaping extreme precipitation variability along Spain's Mediterranean coast (Romero *et al* 1998, Ferreira 2021), we select the d_xZ500, indicative of a pre-trough position east of Spain, as the key circulation metric for reconstructing the 2024 Rx1day in eastern Spain. Among all circulation metrics examined, d_xZ500 most effectively captures the observed precipitation magnitude and dynamically reflects the associated low-level wind anomalies through geostrophic balance (figure S6). In contrast, although vertically integrated zonal moisture transport plays an important role in the event, it contains thermodynamic contributions associated with humidity changes and therefore cannot represent pure dynamical variability. To objectively identify circulation patterns favorable for 2024-like flood events, we further apply SOM analysis based on the d_xZ500. The circulation pattern during the 2024 event is grouped within the fourth SOM node, characterized by a pronounced positive d_xZ500 over the eastern Iberia (figure S7). This node exhibits strong spatial coherence ($r = 0.96$) with the composite of its 469 member days (16.71% of total days) and closely resembles the observed pattern on 29 October 2024 ($r = 0.74$). Mechanistically, this circulation configuration facilitates the low-level advection of warm, moist air from the Mediterranean toward Iberia, where topographic lifting further enhances precipitation (Ferreira 2021). The occurrence frequency of circulation analogs significantly correlated with the fourth SOM pattern exhibits a pronounced seasonal cycle, peaking during late summer and autumn (figure 4(d)), associated with the climatological weakening and equatorward retreat of jet stream, conditions that favor increased meridional flow and probability of COL formation over western Mediterranean (Nieto *et al* 2005).

The ECCA framework based on d_xZ500 analog days is then applied to quantify the contribution of large-scale circulation to the 2024 event. The ensemble mean reconstructed 2024-Rx1day anomaly in eastern Spain of 7.82 mm contributes 31% (interquartile range: 7%–44%) to the total value of 25.33 mm. Although several individual ensemble members reproduce magnitudes comparable to the observed 2024-Rx1day, the ensemble mean remains substantially weaker. This indicates that internal circulation variability alone cannot fully explain the observed intensity, even though large-scale atmospheric dynamics clearly play a key role in shaping the event. In parallel, the dynamically reconstructed Rx1day pattern closely resembles the observed 2024 pattern, exhibiting maxima over eastern Spain with a statistically significant spatial correlation ($r = 0.38$, $p < 0.001$) (figures 4(e) and (f)). Sensitivity experiments that vary both the number of daily analogs and the regularization parameters produce similar spatial features to those in figures 4(e) and (f). Quantitatively, the interquartile range of dynamical contribution narrows slightly to 9%–44% when the number of daily analogs is increased to 20 and to 9%–43% when the regularization parameter is increased to 1, respectively, reinforcing the robustness of the ECCA framework across parameter choices (figure S8).

To further evaluate whether the enhanced dynamical contribution is robust to the hydroclimate in eastern Spain, the ECCA framework is applied to five randomly selected and moderate events (45–55th percentile of Rx1day in 1979–2024) (figure 4(g)). The dynamically induced contributions for the random-event and moderate-event composites are −12% (interquartile range of −27%–16%) and 14% (interquartile range of 1%–25%), respectively, substantially weaker than 31% (7%–44%) estimated for the 2024 event. These results indicate that circulation variability exerts a disproportionately larger influence during the most extreme precipitation events. One possible explanation is that warm-season COL systems are more likely to couple with anomalously warm Mediterranean SSTs, enhancing atmospheric instability and favoring more persistent quasi-stationary circulation structures (Romero *et al* 1998, Nieto *et al* 2005). Notably, applying the ECCA framework to the Turís station yields a substantially smaller dynamical contribution of only 7%–16% (figure S9). Although Turís experienced the most localized precipitation extremes during the 2024 event, limited station record length and the fact that a single station is less representative of the large-scale hydrological response to atmospheric circulation anomalies imply that the ECCA approach is more reasonable for regional-scale precipitation anomalies.

3.3. Large-ensemble attribution of the 2024 extreme precipitation event

To assess the robustness of the attribution framework, we extend the ECCA analysis to the HadGEM3-A-N216 model. Prior to this, the model performance is evaluated. The ensemble mean of the 15-member historical simulations reproduces the

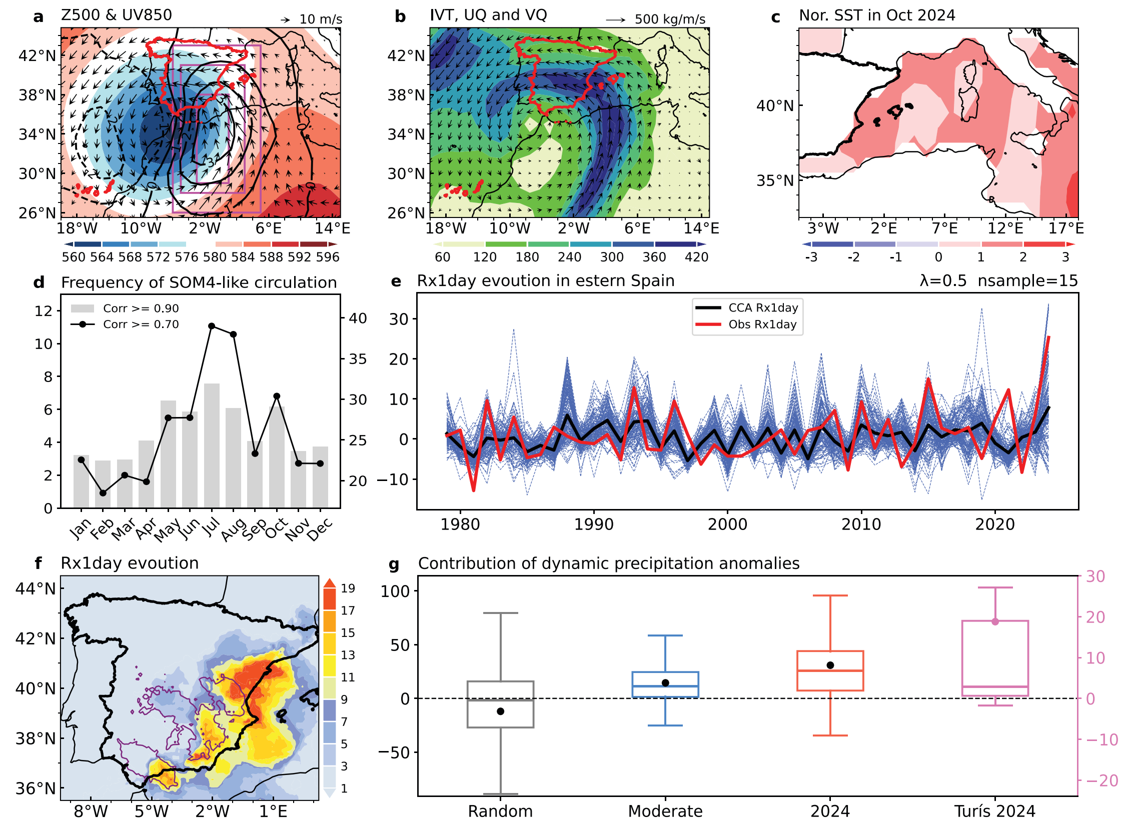

Figure 4. Large-scale circulation and dynamic reconstruction associated with the 2024 Spain precipitation extreme. (a) 500 hPa geopotential height (shading; unit: dagpm), its zonal gradient (contours), and 850 hPa wind (vectors; m s^{-1}) on 29 October 2024. The three magenta boxes indicate three ECCA analysis domains. (b) Same as (a), but for vertically integrated total-column water vapor flux (shading; kg m^{-1} s^{-1}) and its zonal and meridional components (vectors). (c) Same as (b), but for normalized SST in October 2024. (d) Seasonal cycle of the occurrence frequency (d yr^{-1}) of circulation analogs significantly correlated with the fourth SOM pattern during 1979–2024. (e) Observed (red) and dynamically reconstructed (black) Rx1day changes during 1979–2024. The blue dashed lines indicate the values in each ECCA ensemble member. (f) Spatial distribution of dynamically reconstructed 2024 Rx1day (unit: mm; shading). The purple contour outlines the observed Rx1day anomalies of 20 mm d^{-1}. (g) Contribution of the dynamically induced precipitation component for random days, moderate events, and the 2024 event over eastern Spain and at the Turís station (unit: %). The left y-axis denotes the dynamically induced contribution over eastern Spain, while values at the Turís station are shown on the right y-axis.

observed October–November mean precipitation over Spain during 1979–2010 with a statistically significant spatial correlation ($p < 0.01$; figure S10), supporting its reliability for event attribution.

We then explore the 525-member HistExt-2024 ensemble simulated in the HadGEM3-A-N216 model, driven by observed 2024 SST and SIC, to quantify the respective roles of external forcing and internal variability. The externally forced component, represented by the ensemble mean, exhibits broadly positive Rx1day anomalies across central and southern Spain, accounting for approximately 47% (interquartile range: 28%–57%) of the observed anomaly over eastern Spain (figures 5(a) and (d)). However, substantial inter-member spread, particularly over SES, weakens the forced signal, indicating strong modulation by internal variability (figure 5(b)). This is further illustrated by the ten driest and ten wettest ensemble members over eastern Spain, which span a wide range of Rx1day anomalies from near-zero values to extremes comparable to the observed event (figure S11).

In contrast, the internally driven component, the residual between observations (or individual realizations) and the externally forced signal, leads to pronounced wet anomalies over SES, closely resembling the observed spatial distribution and accounting for approximately 53% (interquartile range: 43%–72%) of the total anomaly (figures 5(c) and (d)). To further decompose internal variability, the ECCA framework is applied to the model simulations, reconstructing the internal dynamical component, with the residual representing the thermodynamic contribution (figures 5(d)–(f)). Before ECCA decomposition, we first examine the ensemble members whose circulation patterns most closely resemble the observed 29 October 2024 event. The selected members exhibit SCCs exceeding 0.8 and feature pronounced low-pressure anomalies extending across western Spain and the adjacent Atlantic Ocean (figure S12). The internal dynamical component, associated with pre-trough circulation anomalies, contributes ∼34% (interquartile range: 15%–39%) of the total Rx1day anomaly and successfully captures both the enhanced

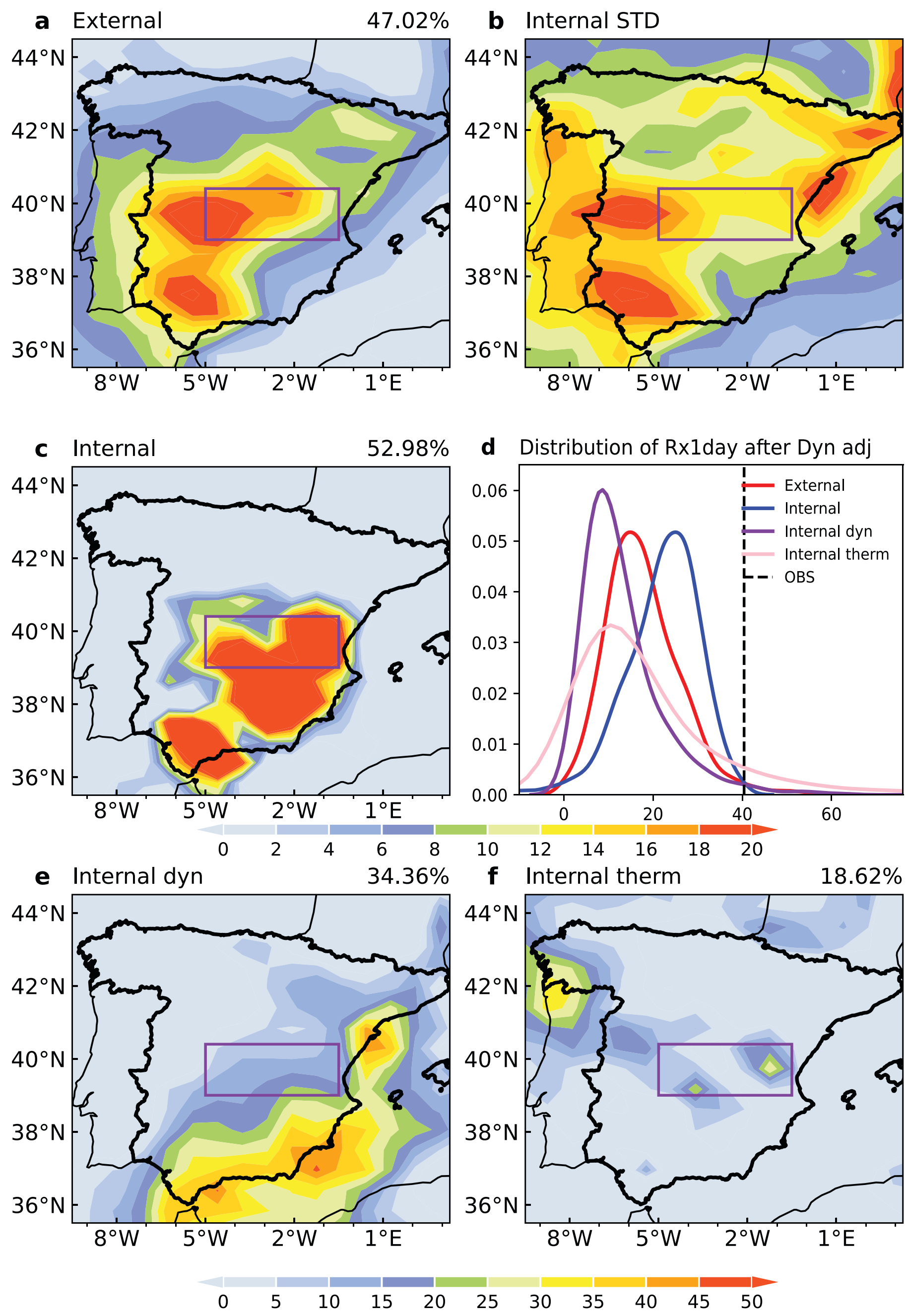

Figure 5. ECCA analysis based on HistExt-2024 large ensemble simulations. (a), (b) Spatial distribution of externally forced October–November Rx1day anomalies (unit: mm day^{-1}) and its standard deviation (STD). The purple box indicates eastern Spain. Numbers in the upper-right corner denote the contribution relative to the 2024 observation in MSWEP. (c), (e) and (f) Same as (a), but for internal, internal dynamical and internal thermodynamic components. (d) Probability density function of the external, internal dynamical and internal thermodynamic components.

precipitation over the southeastern coast and the pre-trough location, with both Rx1day and d_xZ500 fields significantly correlated with observations ($p < 0.05$). The residual internal thermodynamic component contributes a further 19% (interquartile range: 15%–39%). Combined with the externally forced thermodynamic signal, these thermodynamic processes dominate the amplification of the extreme event, accounting for approximately 66%. The probability density functions of the decomposed components reveal distinct characteristics (figure 5(d)). Both external forcing and internal variability could reproduce precipitation magnitudes comparable to the observed 2024 Rx1day, but the internal component exhibits a more positively skewed distribution. Within this, the internal dynamical contribution is concentrated at moderate intensities (0–20 mm d^{-1}), whereas the thermodynamic component shows substantially larger variability and a greater propensity to amplify extremes, likely linked to enhanced precipitation efficiency associated with warm-rain and mixed-phase processes (Gupta et al 2023).

4. Conclusion and discussion

This study investigates the October 2024 extreme precipitation and flooding event in Valencia, Spain, using high-resolution observation, reanalysis products, and large-ensemble simulations. The event, during which 771 mm of precipitation recorded within 24 h on 29 October 2024, ranks among the ten deadliest floods in Europe since 1900. Our analysis reveals that the event was initiated by an anomalously deep upper-level low over southern Spain, accompanied by intense advection of warm, moisture-laden air from the Mediterranean. Orographic lifting along the eastern Iberian coast further intensified ascent and precipitation. At shorter timescales, warm-cloud microphysical processes dominated the instantaneous and convective precipitation, while cold-cloud processes sustained and intensified precipitation during the afternoon of 29 October.

Circulation analog analysis based on d_xZ500 indicates that such a pre-trough configuration accounts for approximately 31% (interquartile range: 7%–44%) of the observed Rx1day anomaly over eastern Spain. Large-ensemble attribution further demonstrates that external forcing and internal variability contribute comparably to the event, accounting for 47% and 53% of the total anomaly, respectively. Decomposition of the internal variability shows that circulation-driven dynamical processes account for 34% of the internally generated anomaly, consistent with the observed interquartile range, while thermodynamic processes contribute the remaining 66%. These thermodynamic contributions, arising from both externally forced warming and internally generated feedbacks, play the dominant role in amplifying the event intensity.

Previous rapid and multi-method attribution studies demonstrated that anthropogenic warming might amplify the 2024 flood event but detected no robust dynamical contribution. By conditioning precipitation on circulation analogs, our framework demonstrates that large-scale atmospheric dynamics played a non-negligible role in shaping the 2024 Spanish event. Nevertheless, several limitations should be acknowledged. First, grid-based precipitation products, including gauge analyses, satellite estimates, and reanalyzes, tend to underestimate localized precipitation extremes and spatial heterogeneity (Hu and Franzke 2020, Peinó *et al* 2024), particularly for sub-daily convective events such as the Valencia precipitation (figure S3). This scale mismatch implies that return periods and circulation diagnostics derived from regional averages differ from those of localized extremes such as Turís. Consistent with previous flood attribution studies, including the July 2021 Henan event (Qin *et al* 2022, Zhao *et al* 2023), our analysis therefore focuses on regional-scale precipitation, while robust attribution of highly localized events remains challenging under current frameworks. Second, the thermodynamic contribution in the ECCA framework is estimated as the residual of circulation-induced anomalies. Any unexplained component of the statistical dynamical adjustment, including unexplained and lagged circulation responses, may be interpreted as thermodynamic variability, implying the estimated 66% thermodynamic contribution should therefore be regarded as an upper bound rather than an exact attribution estimate.

Future developments may help reduce these uncertainties. Kilometer-scale storyline simulations preserve the observed synoptic evolution of an event while perturbing only the thermodynamic background state (Li *et al* 2022, Wang *et al* 2022, Sun *et al* 2024, Ekolu *et al* 2025), providing a physically consistent complement to circulation-conditioned attribution methods for Mediterranean flood events. Meanwhile, emerging machine-learning approaches offer computationally efficient tools for identifying circulation and thermodynamic fingerprints of extremes from large observational and model archives (Madakumbura *et al* 2021, Trok *et al* 2024, Camps-Valls *et al* 2025). Recent studies using convolutional neural networks have successfully captured the dynamical and thermodynamic signatures of historical heatwaves and heavy precipitation events, demonstrating their potential to complement traditional attribution frameworks through efficient, data-driven detection of physically relevant patterns (Trok *et al* 2024). Combining these approaches with circulation-based decomposition frameworks may further improve the physical understanding and near-real-time attribution of future Mediterranean flood disasters.

Acknowledgment

This study is funded by the National Natural Science Foundation of China (42530606 and 42261144687) and the National Key R&D Program of China (Project No. 2025YFF0812000).

Data availability statement

The primarily used MSWEP dataset is derived from www.gloh2o.org/mswep/. Four additional daily precipitation datasets and station-based precipitation observations from AEMET are obtained from https://downloads.psl.noaa.gov/Datasets/cpc_global_precip/, https://data.gesdisc.earthdata.nasa.gov/data/GPM_L3/GPM_3IMERGDF.07/, https://surfobs.climate.copernicus.eu/dataaccess/access_eobs.php#datafiles, https://jra.kishou.go.jp/JRA-3Q/index_en.html and https://opendata.aemet.es/centrodedescargas/productosAEMET. HadISST is free from www.metoffice.gov.uk/hadobs/hadisst. Large-scale atmospheric circulation of ERA5 and

JRA-3Q are available from https://cds.climate.copernicus.eu/datasets/derived-era5-single-levels-daily-statistics?tab=download and https://jra.kishou.go.jp/JRA-3Q/index_en.html. HadGEM3-A-N216 simulation is from https://data.ceda.ac.uk/badc/eucleia/data/EUCLEIA/output/MOHC/HadGEM3-A-N216.

Supplementary data 1 available at: https://doi.org/10.1088/1748-9326/ae8b05/data1.

Author contributions

M.Y. and H.T. conceived and designed the study. M.Y. carried out the data processing, performed the analyses, interpreted the results, and prepared the initial manuscript. H.T. provided guidance and revised the manuscript. G.H. and J.W. contributed with critical comments. All authors have read and approved the final version of the manuscript.

Conflict of interest

The authors declare no competing interests.

ORCID iDs

Mengyuan Yao 0009-0001-8584-280X
Haosu Tang 0000-0002-2924-0126
Gang Huang 0000-0002-8692-7856

References

Barriopedro D, Jiménez-esteve B, Collazo S, Garrido-perez J M, Johnson J E and García-Herrera R 2025 A multimethod attribution analysis of Spain's 2024 extreme precipitation event *Bull. Am. Meteorol. Soc.* **106** E2440–E60

Beck H E, Wood E F, Pan M, Fisher C K, Miralles D G, van Dijk A I J M, McVicar T R and Adler R F 2019 MSWEP V2 global 3-Hourly 0.1° precipitation: methodology and quantitative assessment *Bull. Am. Meteorol. Soc.* **100** 473–500

Blöschl G *et al* 2017 Changing climate shifts timing of European floods *Science* **357** 588–90

Calvo-Sancho C *et al* 2026 Human-induced climate change amplification on storm dynamics in Valencia's 2024 catastrophic flash flood *Nat. Commun.* **17** 1492

Camps-Valls G *et al* 2025 Artificial intelligence for modeling and understanding extreme weather and climate events *Nat. Commun.* **16** 1919

Chang E K M, Guo Y and Xia X 2012 CMIP5 multimodel ensemble projection of storm track change under global warming *J. Geophys. Res. Atmos.* **117** D23118

Charalampous P, Speybroeck N, van Loenhout J A F, Pluen G and Delforge D 2025 The 2024 Spain floods: a call for resilience and the duty of memory *Int. J. Public Health* **70** 1608236

Ciavarella A, Christidis N, Andrews M, Groenendijk M, Rostron J, Elkington M, Burke C, Lott F C and Stott P A 2018 Upgrade of the HadGEM3-A based attribution system to high resolution and a new validation framework for probabilistic event attribution *Weather Clim. Extremes* **20** 9–32

Cornes R C, van der Schrier G, van den Besselaar E J M and Jones P D 2018 An ensemble version of the E-OBS temperature and precipitation data sets *J. Geophys. Res. Atmos.* **123** 9391–409

Cortès M, Turco M, Ward P, Sánchez-espigares J A, Alfieri L and Llasat M C 2019 Changes in flood damage with global warming on the eastern coast of Spain *Nat. Hazards Earth Syst. Sci.* **19** 2855–77

Cramer W *et al* 2018 Climate change and interconnected risks to sustainable development in the Mediterranean *Nat. Clim. Change* **8** 972–80

Durán L, Sanchez E and Yagüe C 2013 Climatology of precipitation over the Iberian central system mountain range *Int. J. Climatol.* **33** 2260–73

Ekolu J *et al* 2025 How could climate change affect the magnitude, duration and frequency of hydrological droughts and floods in West Africa during the 21st century? A storyline approach *J. Hydrol.* **660** 133482

Ferreira R N 2021 Cut-off lows and extreme precipitation in Eastern Spain: current and future climate *Atmosphere* **12** 835

Franch-Pardo I, Fuster Puig P A and Cerdà A 2025 Geospatial technologies in crisis response: analyzing the 2024 floods in Valencia, Spain *Eur. J. Geogr.* **16** 286–97

Grise K M and Davis S M 2020 Hadley cell expansion in CMIP6 models *Atmos. Chem. Phys.* **20** 5249–68

Guerreiro S B, Kilsby C and Fowler H J 2017 Assessing the threat of future megadrought in Iberia *Int. J. Climatol.* **37** 5024–34

Guo R, Deser C, Terray L and Lehner F 2019 Human influence on winter precipitation trends (1921–2015) over North America and Eurasia revealed by dynamical adjustment *Geophys. Res. Lett.* **46** 3426–34

Gupta A K, Deshmukh A, Waman D, Patade S, Jadav A, Phillips V T J, Bansemer A, Martins J A and Gonçalves F L T 2023 The microphysics of the warm-rain and ice crystal processes of precipitation in simulated continental convective storms *Commun. Earth Environ.* **4** 226

Hersbach H *et al* 2020 The ERA5 global reanalysis *Q. J. R. Meteorol. Soc.* **146** 1999–2049

Hu G and Franzke C L E 2020 Evaluation of daily precipitation extremes in reanalysis and gridded observation-based data sets over Germany *Geophys. Res. Lett.* **47** e2020GL089624

Huffman G J *et al* 2024 GPM IMERG final precipitation L3 1 day 0.1 degree x 0.1 degree V07

Insua-Costa D, Lemus-cánovas M, Miguez-macho G and Llasat M C 2021 Climatology and ranking of hazardous precipitation events in the western Mediterranean area *Atmos. Res.* **255** 105521

Japan Meteorological Agency 2023 Japanese reanalysis for three quarters of a century (JRA-3Q)

Johanson C M and Fu Q 2009 Hadley cell widening: model simulations versus observations *J. Clim.* **22** 2713–25

Krichak S O, Breitgand J S, Gualdi S and Feldstein S B 2014 Teleconnection–extreme precipitation relationships over the Mediterranean region *Theor. Appl. Climatol.* **117** 679–92

Kundzewicz Z W, Pińskwar I and Brakenridge G R 2017 Changes in river flood hazard in Europe: a review *Hydrol. Res.* **49** 294–302

Li D, Chen Y, Messmer M, Zhu Y, Feng J, Yin B and Bevacqua E 2022 Compound wind and precipitation extremes across the indo-pacific: climatology, variability, and drivers *Geophys. Res. Lett.* **49** e2022GL098594

Llasat M C, Del Moral A, Cortès M and Rigo T 2021 Convective precipitation trends in the Spanish Mediterranean region *Atmos. Res.* **257** 105581

Madakumbura G D, Thackeray C W, Norris J, Goldenson N and Hall A 2021 Anthropogenic influence on extreme precipitation over global land areas seen in multiple observational datasets *Nat. Commun.* **12** 3944

Masson-Delmotte V *et al* 2021 Climate change 2021: the physical science basis *Contribution of working group I to the sixth assessment report of the intergovernmental panel on climate change* vol 2

Nieto R, Gimeno L, de la Torre L, Ribera P, Gallego D, García-Herrera R, García J A, Nuñez M, Redaño A and Lorente J 2005 Climatological features of cutoff low systems in the northern hemisphere *J. Clim.* **18** 3085–103

Nojarov P 2017 The increase in September precipitation in the Mediterranean region as a result of changes in atmospheric circulation *Meteorol. Atmos. Phys.* **129** 145–56

Omanovic N *et al* 2024 Evaluating the Wegener–Bergeron–Findeisen process in ICON in large-eddy mode with *in situ* observations from the CLOUDLAB project *Atmos. Chem. Phys.* **24** 6825–44

Peinó E, Bech J, Udina M and Polls F 2024 Disentangling satellite precipitation estimate errors of heavy rainfall at daily and sub-daily scale in the Western Mediterranean *Remote Sens.* **16** 457

Peña-Angulo D *et al* 2020 Long-term precipitation in Southwestern Europe reveals no clear trend attributable to anthropogenic forcing *Environ. Res. Lett.* **15** 094070

Polade S D, Gershunov A, Cayan D R, Dettinger M D and Pierce D W 2017 Precipitation in a warming world: assessing projected hydro-climate changes in California and other Mediterranean climate regions *Sci. Rep.* **7** 10783

Qian C, Ye Y, Zhang W and Zhou T 2022 Heavy rainfall event in Mid-August 2020 in Southwestern China: contribution of anthropogenic forcings and atmospheric circulation *Bull. Am. Meteorol. Soc.* **103** S111–S17

Qin H, Yuan W, Wang J, Chen Y, Dai P, Sobel A H, Meng Z and Nie J 2022 Climate change attribution of the 2021 Henan extreme precipitation: impacts of convective organization *Sci. China Earth Sci.* **65** 1837–46

Rayner N, Parker D E, Horton E B, Folland C K, Alexander L V, Rowell D P, Kent E C and Kaplan A 2003 Global analyses of sea surface temperature, sea ice, and night marine air temperature since the late nineteenth century *J. Geophys. Res. Atmos.* **108** 4407

Robinson A, Lehmann J, Barriopedro D, Rahmstorf S and Coumou D 2021 Increasing heat and rainfall extremes now far outside the historical climate *npj Clim. Atmos. Sci.* **4** 45

Romero R, Ramis C, Alonso S, Doswell C A and Stensrud D J 1998 Mesoscale model simulations of three heavy precipitation events in the Western Mediterranean region *Mon. Weather Rev.* **126** 1859–81

Seneviratne S I *et al* 2023 Weather and climate extreme events in a changing climate *Climate Change 2021—The Physical Science Basis: Working Group I Contribution to the Sixth Assessment Report of the Intergovernmental Panel on Climate Change* pp 1513–766

Shi R, Lu C, Xu W and Luo Y 2025 A global view on microphysical discriminations between heavier and lighter convective rainfall *Commun. Earth Environ.* **6** 511

Singh J, Sippel S and Fischer E M 2023 Circulation dampened heat extremes intensification over the Midwest USA and amplified over Western Europe *Commun. Earth Environ.* **4** 432

Smoliak B V, Wallace J M, Lin P and Fu Q 2015 Dynamical adjustment of the northern hemisphere surface air temperature field: methodology and application to observations *J. Clim.* **28** 1613–29

Sun W, Li J, Yu R, Li N and Zhang Y 2024 Exploring changes of precipitation extremes under climate change through global variable-resolution modeling *Sci. Bull.* **69** 237–47

Swales D, Alexander M and Hughes M 2016 Examining moisture pathways and extreme precipitation in the U.S. Intermountain West using self-organizing maps *Geophys. Res. Lett.* **43** 1727–35

Tapiador F J, Sánchez E and Gaertner M A 2007 Regional changes in precipitation in Europe under an increased greenhouse emissions scenario *Geophys. Res. Lett.* **34** L02701

Tarín-Carrasco P, Petrova D, Chica-Castells L, Lukovic J, Rodó X and Cvijanovic I 2025 Assessment of future precipitation changes in mediterranean climate regions from CMIP6 ensemble *Int. J. Climatol.* **45** e70039

Tramblay Y and Somot S 2018 Future evolution of extreme precipitation in the Mediterranean *Clim. Change* **151** 289–302

Treppiedi D, Cipolla G and Noto L 2022 Convective precipitation over a Mediterranean area: from identification to trend analysis starting from high-resolution rain gauges data *Int. J. Climatol.* **43** 293–313

Trok J T, Barnes E A, Davenport F V and Diffenbaugh N S 2024 Machine learning–based extreme event attribution *Sci. Adv.* **10** eadl3242

Wang J, Chen Y, Nie J, Yan Z, Zhai P and Feng J 2022 On the role of anthropogenic warming and wetting in the July 2021 Henan record-shattering rainfall *Sci. Bull.* **67** 2055–9

Xie P, Chen M and Shi W 2010 CPC unified gauge-based analysis of global daily precipitation *24th Conf. on Hydrology* (American Meteorological Society (AMS)) vol 2

Yao M, Tang H and Huang G 2026 Anthropogenic warming and ocean variability exacerbated spring 2024 compound floods in Central Asia *J. Geophys. Res. Atmos.* **131** e2025JD045602

Zhang S, Chen Y, Luo Y, Liu B, Ren G, Zhou T, Martinez-villalobos C and Chang M 2022 Revealing the circulation pattern most conducive to precipitation extremes in henan province of North China *Geophys. Res. Lett.* **49** e2022GL098034

Zhang X, Zhou T, Zhang W, Ren L, Jiang J, Hu S, Zuo M, Zhang L and Man W 2023 Increased impact of heat domes on 2021-like heat extremes in North America under global warming *Nat. Commun.* **14** 1690

Zhao D, Xu H, Wang H, Yu Y, Duan Y and Chen L 2023 Quantitative attribution of historical anthropogenic warming on the extreme rainfall event over Henan in July 2021 *Environ. Res. Lett.* **18** 104037